

Hemodynamic and metabolic diffuse optical monitoring in a mouse model of hindlimb ischemia

Rickson C. Mesquita,^{1,*} Nicolas Skuli,^{2,3} Meeri N. Kim,¹ Jiaming Liang,^{1,4}
Steve Schenkel,¹ Amar J. Majmundar,^{2,5} M. Celeste Simon,^{2,3,6} and Arjun G. Yodh¹

¹Department of Physics & Astronomy, University of Pennsylvania, Philadelphia, PA 19104, USA

²Abramson Family Cancer Research Institute, University of Pennsylvania, Philadelphia, PA 19104, USA

³Howard Hughes Medical Institute, University of Pennsylvania, Philadelphia, PA 19104, USA

⁴School of Life Science and Technology, Xi'an Jiaotong University, Xi'an 710049, China

⁵School of Medicine, University of Pennsylvania, Philadelphia, PA 19104, USA

⁶Department of Cell and Developmental Biology, University of Pennsylvania, Philadelphia, PA 19104, USA

*rickson@nmr.mgh.harvard.edu

Abstract: Murine hindlimb ischemia is a useful model for investigation of the mechanisms of peripheral arterial disease and for understanding the role of endothelial cells and generic factors affecting vascular regeneration or angiogenesis. To date, important research with these models has explored tissue reperfusion following ischemia with Laser Doppler methods, methods which provide information about superficial (~mm) vascular regeneration. In this work, we employ diffuse correlation spectroscopy (DCS) and diffuse optical spectroscopy (DOS) in mice after hindlimb ischemia. We hypothesize that vascular re-growth is not uniform in tissue, and therefore, since diffuse optical methods are capable of probing deep tissues, that the diffuse optics approach will provide a more complete picture of the angiogenesis process throughout the whole depth profile of the limb. Besides increased depth penetration, the combined measurements of DCS and DOS enable all-optical, noninvasive, longitudinal monitoring of tissue perfusion and oxygenation that reveals the interplay between these hemodynamic parameters during angiogenesis. Control mice were found to reestablish 90% of perfusion and oxygen consumption during this period, but oxygen saturation in the limb only partially recovered to about 30% of its initial value. The vascular recovery of mice with endothelial cell-specific deletion of HIF-2 α was found to be significantly impaired relative to control mice, indicating that HIF-2 α is important for endothelial cell functions in angiogenesis. Comparison of DOS/DCS measurements to parallel measurements in the murine models using Laser Doppler Flowmetry reveal differences in the reperfusion achieved by superficial versus deep tissue during neoangiogenesis; findings from histological analysis of blood vessel development were further correlated with these differences. In general, the combination of DCS and DOS enables experimenters to obtain useful information about oxygenation, metabolism, and perfusion throughout the limb. The results establish diffuse optics as a practical noninvasive method to evaluate the role of transcription factors, such as the endothelial cell-specific HIF-2 α , in genetic ally modified mice.

©2010 Optical Society of America

OCIS codes: (170.3880) Medical and biological imaging; (170.1420) Biology; (170.3660) Light propagation in tissues; (170.5380) Physiology.

References and links

1. P. Carmeliet, "Angiogenesis in life, disease and medicine," *Nature* **438**(7070), 932–936 (2005).
2. M. M. Hickey, and M. C. Simon, "Regulation of angiogenesis by hypoxia and hypoxia-inducible factors," *Curr. Top. Dev. Biol.* **76**, 217–257 (2006).

3. K. L. Covello, and M. C. Simon, "HIFs, hypoxia, and vascular development," *Curr. Top. Dev. Biol.* **62**, 37–54 (2004).
4. B. Zhou, M. C. Poon, W. T. Pu, and Z. C. Han, "Therapeutic neovascularization for peripheral arterial diseases: advances and perspectives," *Histol. Histopathol.* **22**(6), 677–686 (2007).
5. J. A. Bertout, S. A. Patel, and M. C. Simon, "The impact of O₂ availability on human cancer," *Nat. Rev. Cancer* **8**(12), 967–975 (2008).
6. M. Heil, I. Eitenmüller, T. Schmitz-Rixen, and W. Schaper, "Arteriogenesis versus angiogenesis: similarities and differences," *J. Cell. Mol. Med.* **10**(1), 45–55 (2006).
7. D. Scholz, T. Ziegelhoeffer, A. Helisch, S. Wagner, C. Friedrich, T. Podzuweit, and W. Schaper, "Contribution of arteriogenesis and angiogenesis to postocclusive hindlimb perfusion in mice," *J. Mol. Cell. Cardiol.* **34**(7), 775–787 (2002).
8. A. Helisch, S. Wagner, N. Khan, M. Drinane, S. Wolfram, M. Heil, T. Ziegelhoeffer, U. Brandt, J. D. Pearlman, H. M. Swartz, and W. Schaper, "Impact of mouse strain differences in innate hindlimb collateral vasculature," *Arterioscler. Thromb. Vasc. Biol.* **26**(3), 520–526 (2005).
9. T. Couffinhal, M. Silver, L. P. Zheng, M. Kearney, B. Witzembichler, and J. M. Isner, "Mouse model of angiogenesis," *Am. J. Pathol.* **152**(6), 1667–1679 (1998).
10. E. Deindl, I. Buschmann, I. E. Hoefer, T. Podzuweit, K. Boengler, S. Vogel, N. van Royen, B. Fernandez, and W. Schaper, "Role of ischemia and of hypoxia-inducible genes in arteriogenesis after femoral artery occlusion in the rabbit," *Circ. Res.* **89**(9), 779–786 (2001).
11. G. L. Wang, and G. L. Semenza, "Purification and characterization of hypoxia-inducible factor 1," *J. Biol. Chem.* **270**(3), 1230–1237 (1995).
12. H. Tian, S. L. McKnight, and D. W. Russell, "Endothelial PAS domain protein 1 (EPAS1), a transcription factor selectively expressed in endothelial cells," *Genes Dev.* **11**(1), 72–82 (1997).
13. I. E. Hoefer, N. van Royen, I. R. Buschmann, J. J. Piek, and W. Schaper, "Time course of arteriogenesis following femoral artery occlusion in the rabbit," *Cardiovasc. Res.* **49**(3), 609–617 (2001).
14. M. Bosch-Marce, H. Okuyama, J. B. Wesley, K. Sarkar, H. Kimura, Y. V. Liu, H. Zhang, M. Strazza, S. Rey, L. Savino, Y. F. Zhou, K. R. McDonald, Y. Na, S. Vandiver, A. Rabi, Y. Shaked, R. Kerbel, T. Lavalley, and G. L. Semenza, "Effects of aging and hypoxia-inducible factor-1 activity on angiogenic cell mobilization and recovery of perfusion after limb ischemia," *Circ. Res.* **101**(12), 1310–1318 (2007).
15. K. R. Forrester, C. Stewart, J. Tulip, C. Leonard, and R. C. Bray, "Comparison of laser speckle and laser Doppler perfusion imaging: measurement in human skin and rabbit articular tissue," *Med. Biol. Eng. Comput.* **40**(6), 687–697 (2002).
16. T. Durduran, R. Choe, W. B. Baker, and A. G. Yodh, "Diffuse optics for tissue monitoring and tomography," *Rep. Prog. Phys.* **73**(7), 076701 (2010).
17. M. Solonenko, R. Cheung, T. M. Busch, A. Kachur, G. M. Griffin, T. Vulcan, T. C. Zhu, H. W. Wang, S. M. Hahn, and A. G. Yodh, "In vivo reflectance measurement of optical properties, blood oxygenation and motexafin lutetium uptake in canine large bowels, kidneys and prostates," *Phys. Med. Biol.* **47**(6), 857–873 (2002).
18. H.-W. Wang, E. Rickter, M. Yuan, E. P. Wileto, E. Glatstein, A. Yodh, and T. M. Busch*, "Effect of Photosensitizer Dose on Fluence Rate Responses to Photodynamic Therapy," *Photochem. Photobiol.* **83**(5), 1040–1048 (2007).
19. D. A. Boas, L. E. Campbell, and A. G. Yodh, "Scattering and imaging with diffusing temporal field correlations," *Phys. Rev. Lett.* **75**(9), 1855–1858 (1995).
20. D. A. Boas, and A. G. Yodh, "Spatially varying dynamical properties of turbid media probed with diffusing temporal light correlation," *J. Opt. Soc. Am. A* **14**(1), 192–215 (1997).
21. G. Q. Yu, T. F. Floyd, T. Durduran, C. Zhou, J. J. Wang, J. A. Detre, and A. G. Yodh, "Validation of diffuse correlation spectroscopy for muscle blood flow with concurrent arterial spin labeled perfusion MRI," *Opt. Express* **15**(3), 1064–1075 (2007).
22. T. Durduran, C. Zhou, E. M. Buckley, M. N. Kim, G. Yu, R. Choe, J. W. Gaynor, T. L. Spray, S. M. Durning, S. E. Mason, L. M. Montenegro, S. C. Nicolson, R. A. Zimmerman, M. E. Putt, J. J. Wang, J. H. Greenberg, J. A. Detre, A. G. Yodh, and D. J. Licht, "Optical measurement of cerebral hemodynamics and oxygen metabolism in neonates with congenital heart defects," *J. Biomed. Opt.* **15**(3), 037004 (2010).
23. M. N. Kim, T. Durduran, S. Frangos, B. L. Edlow, E. M. Buckley, H. E. Moss, C. Zhou, G. Yu, R. Choe, E. Maloney-Wilensky, R. L. Wolf, M. S. Grady, J. H. Greenberg, J. M. Levine, A. G. Yodh, J. A. Detre, and W. A. Kofke, "Noninvasive measurement of cerebral blood flow and blood oxygenation using near-infrared and diffuse correlation spectroscopies in critically brain-injured adults," *Neurocrit. Care* **12**(2), 173–180 (2010).
24. C. Zhou, S. A. Eucker, T. Durduran, G. Yu, J. Ralston, S. H. Friess, R. N. Ichord, S. S. Margulies, and A. G. Yodh, "Diffuse optical monitoring of hemodynamic changes in piglet brain with closed head injury," *J. Biomed. Opt.* **14**(3), 034015 (2009).
25. N. Skuli, L. Liu, A. Runge, T. Wang, L. Yuan, S. Patel, L. Iruela-Arispe, M. C. Simon, and B. Keith, "Endothelial deletion of hypoxia-inducible factor-2 (HIF-2) alters vascular function and tumor angiogenesis," *Blood* **114**(2), 469–477 (2009).
26. V. E. Papaioannou, and J. G. Fox, "Efficacy of tribromoethanol anesthesia in mice," *Lab. Anim. Sci.* **43**(2), 189–192 (1993).
27. A. Limbourg, T. Korff, L. C. Napp, W. Schaper, H. Drexler, and F. P. Limbourg, "Evaluation of postnatal arteriogenesis and angiogenesis in a mouse model of hind-limb ischemia," *Nat. Protoc.* **4**(12), 1737–1748 (2009).
28. S. F. Winter, V. D. Acevedo, R. D. Gangula, K. W. Freeman, D. M. Spencer, and N. M. Greenberg, "Conditional activation of FGFR1 in the prostate epithelium induces angiogenesis with concomitant differential regulation of Ang-1 and Ang-2," *Oncogene* **26**(34), 4897–4907 (2007).

29. S. R. Arridge, M. Cope, and D. T. Delpy, "The theoretical basis for the determination of optical pathlengths in tissue: temporal and frequency analysis," *Phys. Med. Biol.* **37**(7), 1531–1560 (1992).
30. S. Prah, Optical properties spectra, <http://omlc.ogi.edu/spectra/index.html>
31. S. Takatani, and M. D. Graham, "Theoretical analysis of diffuse reflectance from a two-layer tissue model," *IEEE Trans. Biomed. Eng.* **26**(12), 656–664 (1979).
32. J. A. Nelder, and R. Mead, "A simplex method for function minimization," *Comput. J.* **7**, 308–313 (1965).
33. H. W. Wang, J. C. Finlay, K. Lee, T. C. Zhu, M. E. Putt, E. Glatstein, C. J. Koch, S. M. Evans, S. M. Hahn, T. M. Busch, and A. G. Yodh, "Quantitative comparison of tissue oxygen and motexafin lutetium uptake by ex vivo and noninvasive in vivo techniques in patients with intraperitoneal carcinomatosis," *J. Biomed. Opt.* **12**(3), 034023 (2007).
34. J. P. Culver, T. Durduran, D. Furuya, C. Cheung, J. H. Greenberg, and A. G. Yodh, "Diffuse optical tomography of cerebral blood flow, oxygenation, and metabolism in rat during focal ischemia," *J. Cereb. Blood Flow Metab.* **23**(8), 911–924 (2003).
35. J. Mayhew, D. Johnston, J. Martindale, M. Jones, J. Berwick, and Y. Zheng, "Increased oxygen consumption following activation of brain: theoretical footnotes using spectroscopic data from barrel cortex," *Neuroimage* **13**(6), 975–987 (2001).
36. D. A. Boas, G. Strangman, J. P. Culver, R. D. Hoge, G. Jaszczewski, R. A. Poldrack, B. R. Rosen, and J. B. Mandeville, "Can the cerebral metabolic rate of oxygen be estimated with near-infrared spectroscopy?" *Phys. Med. Biol.* **48**(15), 2405–2418 (2003).
37. D. A. Boas, J. P. Culver, J. J. Stott, and A. K. Dunn, "Three dimensional Monte Carlo code for photon migration through complex heterogeneous media including the adult human head," *Opt. Express* **10**(3), 159–170 (2002).
38. L. Gagnon, M. Desjardins, J. Jehanne-Lacasse, L. Bherer, and F. Lesage, "Investigation of diffuse correlation spectroscopy in multi-layered media including the human head," *Opt. Express* **16**(20), 15514–15530 (2008).
39. P. Carmeliet, "Mechanisms of angiogenesis and arteriogenesis," *Nat. Med.* **6**(4), 389–395 (2000).
40. W. Schaper, "Collateral circulation: past and present," *Basic Res. Cardiol.* **104**(1), 5–21 (2009).
41. L. H. Gray, and J. M. Steadman, "Determination of the oxyhaemoglobin dissociation curves for mouse and rat blood," *J. Physiol.* **175**, 161–171 (1964).
42. K. Schmidt-Neilsen, and J. L. Larimer, "Oxygen dissociation curves of mammalian blood in relation to body size," *Am. J. Physiol.* **195**(2), 424–428 (1958).
43. H. W. Wang, M. E. Putt, M. J. Emanuele, D. B. Shin, E. Glatstein, A. G. Yodh, and T. M. Busch, "Treatment-induced changes in tumor oxygenation predict photodynamic therapy outcome," *Cancer Res.* **64**(20), 7553–7561 (2004).
44. A. Matsumoto, S. Matsumoto, A. L. Sowers, J. W. Koscielniak, N. J. Trigg, P. Kuppusamy, J. B. Mitchell, S. Subramanian, M. C. Krishna, and K. I. Matsumoto, "Absolute oxygen tension (pO₂) in murine fatty and muscle tissue as determined by EPR," *Magn. Reson. Med.* **54**(6), 1530–1535 (2005).

1. Introduction

Angiogenesis is the process by which new blood vessels develop from pre-existing vessels [1]. This physiological response helps preserve tissue integrity and/or function in settings of local hypoxia, or reduced O₂ availability [2]. Angiogenic responses can arise in a variety of hypoxic contexts, ranging from normal embryonic development [3] to pathologies such as peripheral arterial disease (PAD) [4] and solid tumors [5].

Ligation of the femoral artery in mice is an established approach to model angiogenesis and has provided a deeper understanding of responses to limb ischemia. This model of hindlimb ischemia is useful for identifying new targets and testing new therapies. After femoral artery ligation, the limb displays a severe decrease in blood flow, generally less than 20% of the flow in the contralateral limb. In response to this ischemia, a vascular response develops marked by the formation of new blood vessels (i.e., neoangiogenesis) in the thigh and calf muscles.

Ligation of the femoral artery also induces another vascular response known as arteriogenesis. In this process, collateral vessels of the femoral artery exhibit a sudden increase in blood flow in addition to other hemodynamic changes. Moreover, these vessels undergo remodeling and growth into parallel conductance vessels, thereby establishing a collateral circuit [6]. Normal blood flow in ischemic hindlimb is restored gradually in the month following ligation, although the degree of recovery varies with mouse strain [7,8].

Therefore, the murine femoral artery ligation model has provided a system to investigate how specific factors and cell types (such as endothelial cells) contribute to vascular regeneration. The resulting information has clear implications for better understanding of diseases such as PAD. By employing genetically engineered mice, studies have shown that recovery of tissue perfusion by revascularization/neoangiogenesis requires appropriate growth factors to orchestrate recruitment, migration, proliferation, and differentiation of vascular

endothelial cells, which are, in part, responsible for forming the vascular network [9,10]. In addition to soluble factors, endothelial cells can respond directly to physiological cues such as O₂ availability in culture. However, the details about how reduced O₂ availability influences endothelial cell functions *in vivo* are not well understood.

The cellular response to hypoxia is mediated by Hypoxia Inducible Factors (HIFs), which are transcription factors belonging to the basic Helix Loop Helix (bHLH)/Per-Arnt/Ahr-Sim (PAS) protein family. HIFs promote adaptation to hypoxia through regulation of more than 150 genes involved in angiogenesis, metabolism, cell proliferation and cell migration [1]. Two major HIF- α subunits mediate cellular adaptation to hypoxia: HIF-1 α [11] and HIF-2 α (also known as EPAS-1) [12]. While HIF-1 α is broadly expressed, HIF-2 α expression is restricted to select cell populations such as the vascular endothelium. Moreover, HIF-2 α is known to regulate several angiogenic factors in endothelial cells, suggesting that this subunit may regulate important endothelial cell functions during angiogenic responses. Based on these observations, HIF-2 α deficiency can impair hypoxic adaptation of endothelial cells, and can lead to modulation in vascular regeneration and adaptation of mice with specific deletion of HIF-2 α in endothelial cells.

The role of HIFs in vascular regeneration and tissue reperfusion has been studied with microspheres [10,13], Laser Doppler Flowmetry (LDF), and Laser Speckle Imaging (LSI) methods [9,14]. LDF remains the standard technique in animal models of PAD and “normal” angiogenesis. Laser Doppler perfusion imaging (LDI) is a recent advancement of the LDF technique that provides a two-dimensional image of tissue perfusion without sample contact. However, the technique has long scan times, low image resolution, and requires that the sample remain still during the entire scan [15].

Translation of diffuse optical methods to angiogenesis animal models may lead to a more robust and complete characterization of the tissue reperfusion process. While useful information about blood flow in the superficial tissues can be obtained with LDF or LDI methods (~mm from the skin), diffuse optical techniques provide assessment to oxygenation and metabolic processes of the microvasculature of deeper tissues (~cm from the skin). Therefore, unlike current available techniques that assess superficial tissue hemodynamics only, diffuse optical techniques permit characterization across the whole tissue probed by performing measurements at different source-detector separations, thereby providing a noninvasive diagnostic of tissue dynamics at both hemodynamic and metabolic levels.

The methodology employs photons in the near-infrared range (650-900 nm) that diffuse through tissue and can be detected millimeters to centimeters away from the source [16]. The absorption spectra of water, oxy- (HbO₂), and deoxy-hemoglobin (Hb) provides access to physiological parameters such as blood oxygen saturation and hemoglobin concentration. The present work employs two diffuse optical techniques: Diffuse Optical Spectroscopy (DOS) and Diffuse Correlation Spectroscopy (DCS). DOS probes tissue absorption and reduced scattering spectra using a lamp and an imaging spectrograph [17,18]. By projecting the dispersed light from the diffraction grating onto a CCD camera, the spectral distribution of the detected light is accessed and is used to derive absorption and scattering coefficients of the tissue. The latter coefficient provides an estimate of the size distribution and density of the scatterers, and the former provides information about absolute hemoglobin concentrations.

Diffuse Correlation Spectroscopy (DCS) is a diffuse optical technique sensitive to the motions of scatterers in tissue, such as red blood cells [19,20]. In DCS, sensitivity to blood flow is derived from the decay rate of the temporal intensity autocorrelation function of the detected light. Although absolute measurements of perfusion are difficult to obtain, DCS readily provides information about relative variation of microvascular perfusion. The technique has been validated both in animals and in humans, including comparison with other experimental techniques such as arterial spin-labeled MRI (ASL-MRI) [21,22], Xenon-CT [23], and fluorescent microspheres [24]. Both DCS and DOS share common advantages such as portability, high temporal resolution, and the ability to probe deep tissues noninvasively.

In this study we combined DCS and DOS methods to determine longitudinal blood flow and oxygenation responses in a mouse hindlimb ischemia model. Perfusion and oxygenation

were measured in the left hindlimb before and after femoral artery ligation and were then compared to similar measurements of the contralateral control limb. Mice were followed periodically for four weeks after surgery to monitor the revascularization process initiated by angiogenesis. To evaluate whether diffuse optics can feasibly distinguish between mice with different angiogenic properties, mice with endothelial-specific deletion of HIF-2 α were evaluated relative to control mice. Multiple source-detector separations were used to investigate differences across the cross-section of the limb. In addition, DCS-based measurements of perfusion ratio were compared to relative blood flow measurements performed with LDF, and a significant correlation between the two techniques was found for the pre-surgery/post-surgery perfusion ratio of the two hindlimbs. In summary, our results demonstrate that DCS can reliably distinguish between mice with different angiogenic properties, and that deep tissue probes add important new information about vessel formation in the limb, and that combined measurements of DCS and DOS provide more comprehensive information about tissue oxygen saturation, total hemoglobin concentration, perfusion, and metabolic rate of oxygen consumption in murine models.

2. Methods

2.1 Animal preparation and protocol

We assessed blood flow and oxygenation values before and after femoral artery ligation in 42 mice, which ranged from 8 to 10 months old and from 25 to 30 g. All mice were on a mixed Sv-129/C57-B16 genetic background. The animals were of two different genotypes: 20 had HIF-2 α deleted in endothelial cells (KO mice), while the remaining mice were controls. Endothelial specific deletion of HIF-2 α was generated by first breeding the HIF-2 α ^{fl/fl} mice with transgenic mice expressing Cre recombinase under the VE-cadherin promoter, as previously described [25]. HIF-2 α control and KO mice were distinguished using a multiplex Polymerase Chain Reaction (PCR) approach. All animal experiments were conducted in accordance with National Institutes of Health guidelines for use and care of live animals and were approved by the University of Pennsylvania Institutional Animal Care and Use Committee (IACUC). Animals were anesthetized using Avertin (2, 2, 2-Tribromoethanol, SIGMA) prepared as a 1.2% solution at a dosage of 0.2 ml/10g body weight, which approximates 240 mg/kg [26].

Unilateral femoral artery ligation was performed as described in [9]. Follow-up hemodynamic measurements were carried out postoperatively once a week over 4 weeks. Due to the age and severity of the procedure, only 21 mice survived the entire period (10 KO and 11 controls). After 28 days, the remaining animals were sacrificed, and the tissues were processed for analysis. Tissue sampling and morphometric analysis of collateral artery growth and capillary formation were performed as described in [27,28]. Briefly, vasculature was perfused with Phosphate Buffered Saline (PBS) followed by 4% paraformaldehyde. Adductor muscles were dissected, cryopreserved, sectioned, and mounted in Fluoromount-G media (SouthernBiotech) for immunohistochemistry staining with Rhodamine (Griffonia simplicifolia) Lectin (Vector Laboratories). Image analyses and quantifications were performed using a Leica 500 microscope as well as Image J and Metamorph software (Molecular Devices).

Blood vessels/capillaries in tissue sections from control and KO mice were visualized using lectin staining. The number of vessels and the vasculature area were measured, as described in [28]. Vascular area was defined as the combined area of Rhodamine-labeled vessels plus lumens in 5 independent fields, expressed as a percentage of the total image area.

2.2 Oxygenation measurements and data analysis

The DOS system was composed of a 250 W tungsten-halogen light source (TS-428, PI Acton, MA), a spectrometer (SP-150, Acton Research, MA), and a 16-bit, back-illuminated CCD camera (PIXIS: 400BR, Princeton Instruments, NJ). The exposure time of the camera was set to 150 ms. The optical probe consisted of a single source- and ten detection-fibers (each with

a core diameter of 400 μm) spaced non-uniformly. The source-detector (SD) separations were 0.6, 1.2, 1.8, 2.4, 3.0, 4.0, 5.0, 6.0, 8.0 and 10 mm. The probe was positioned longitudinally on each hindlimb, with the top of the probe slightly above the femoral artery location where surgery was performed (Fig. 1).

The analytical solution of the photon diffusion equation for a slab geometry with extrapolated zero boundary condition in the continuous-wave domain was used to fit the measured data in the wavelength range from 550 to 900 nm. In this case, the fluence rate Φ is given by [16,29]:

$$\Phi(r, t) = \frac{v}{4\pi D} \sum_m \left(\frac{e^{-k_0 \cdot r_{+,m}}}{r_{+,m}} - \frac{e^{-k_0 \cdot r_{-,m}}}{r_{-,m}} \right), \quad (1)$$

where v is the velocity of light in the tissue, $D = D(r) = v / [3(\mu'_s + \mu_a)]$ is the light diffusion coefficient, $k_0^2 = v\mu_a / D$, and μ_a and μ'_s are the tissue absorption and reduced scattering coefficients, respectively. In addition, $r_{\pm,m} = \sqrt{\rho^2 + (z - z_{\pm,m})^2}$, $z_{+,m} = 2m(d + 2L_s) + l_t$, and $z_{-,m} = 2m(d + 2L_s) - 2L_s - l_t$, where (ρ, z) are the cylindrical coordinates at point r , d is the slab thickness, and l_t and L_s are the location of the real and image sources, respectively. In this work, we considered the first 10 terms of the sum in Eq. (1); subsequent terms were very small. The slab thickness was fixed at 12 mm, which was the average thickness (averaged over 10 animals) measured in the region covered by the probe.

The tissue optical properties were assumed to have the following spectral forms:

$$\mu'_s(\lambda) = A\lambda^{-b} \quad \text{and} \quad \mu_a(\lambda) = \sum_i \varepsilon_i(\lambda) \cdot c_i. \quad (2)$$

The scattering parameters A and b are related to scatterer size distribution and number density. For absorption, ε_i and c_i are the extinction coefficient (wavelength dependent) and the concentration of the i^{th} chromophore, respectively. The main tissue chromophores are oxy-hemoglobin (HbO_2), deoxy-hemoglobin (Hb), and water, and their extinction coefficients were obtained from the literature [30,31]. A nonlinear inversion algorithm based on the Nelder-Mead algorithm [32] was used to recover the absolute optical properties from reflection data. From the absorption coefficient we extracted absolute HbO_2 and Hb concentrations (c_{HbO_2} and c_{Hb} , respectively) using Eq. (2), and then we calculated the total hemoglobin concentration ($\text{THC} = c_{\text{HbO}_2} + c_{\text{Hb}}$) and blood oxygen saturation ($S_{\text{tO}_2} = c_{\text{HbO}_2} / \text{THC}$) of the tissue.

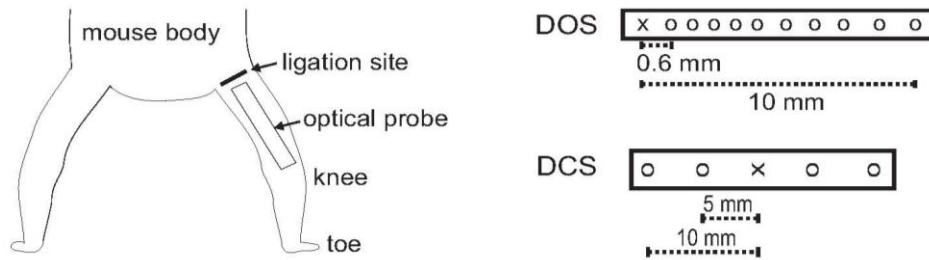


Fig. 1. Schematic diagram showing the position of the optical probe on the mouse hindlimb. The design of the probe is shown in the right side for both DOS (top) and DCS (bottom).

All spectra were calibrated by the emission spectrum of the white-light source (collected with an integrating sphere), and then dark-count levels were subtracted [33]. Signals from the shortest source-detector separation were not used due to sporadic light leakage. The other source-detector pair intensities were normalized by the second shortest separation, and the final spectra were then compared with the analytical solution [Eq. (1)].

For each measurement, we collected data at nine different locations along both the ligated and normal hindlimbs. The hemodynamic parameters for each hindlimb of each mouse at every time point were estimated from the mean of the nine different locations.

2.3 Perfusion measurements and data analysis

DCS measurements were performed with a home-built instrument containing two continuous wave, long coherent length (> 5 m), 785 nm lasers (CrystaLaser Inc., Reno, NV), and eight avalanche photodiodes (PerkinElmer, Canada). One 8-channel autocorrelator board (Correlator.com, Bridgewater, NJ) was employed to compute the intensity temporal correlation function for an integration time of 500 ms. Data were collected simultaneously in both limbs, with four detectors distributed symmetrically along one single source positioned at the center for each limb. The source-detector separations were 0.5 and 1.0 cm. The DCS probe was positioned similar to the DOS probe, with the top of the probe slightly above the femoral artery location where surgery was performed (Fig. 1).

For data analysis, the solution of the photon correlation diffusion equation in a homogeneous slab geometry with extrapolated zero boundary conditions was used to derive the electric field temporal autocorrelation function, $G_1(\tau) = \langle E^*(\tau=0)E(\tau) \rangle$ [16]:

$$G_1(\tau) = \frac{3\mu_s'}{4\pi} \sum_m \left(\frac{e^{-K(\tau)r_{+,m}}}{r_{+,m}} - \frac{e^{-K(\tau)r_{-,m}}}{r_{-,m}} \right), \quad (3)$$

where $K^2(t, \tau) = \left(\mu_a(t, \lambda) + \frac{1}{3} \alpha \mu_s' k_0^2 \langle \Delta r^2(t, \tau) \rangle \right) / (3\mu_s')$, τ is the correlation time, k_0 is the wave vector, α represents the fraction of photon scattering events in the tissue, and $\langle \Delta r^2(t, \tau) \rangle$ is the mean-square displacement of the scattering particles in time τ ; the brackets $\langle \rangle$ denote time averages (for experiments) or ensemble averages (for calculations). In this work, we used the Brownian motion model in Eq. (3) to approximate the mean-square particle displacement, i.e., $\langle \Delta r^2(t, \tau) \rangle = 6D_B\tau$, where D_B represents the effective diffusion coefficient of the moving scatterers. The measurement of the normalized intensity autocorrelation function, $g_2(\tau) = \langle I^*(\tau=0)I(\tau) \rangle / \langle I(\tau=0) \rangle^2$, can be related to the normalized electric field correlation function, $g_1(\tau) = \langle E^*(\tau=0)E(\tau) \rangle / |E(\tau=0)|^2$, by the Siegert relation:

$$g_2(r, t, \tau) = 1 + \beta |g_1(r, t, \tau)|^2. \quad (4)$$

Here, β is a parameter that depends on the source coherence, detection optics, and other external factors. In order to estimate relative blood flow from the DCS data, we fit the measured intensity autocorrelation functions to Eq. (4) to extract both β and a blood flow index (BFI), defined as $BFI(t) \equiv \alpha D_B(t)$. The blood flow index has been demonstrated to be proportional to blood flow in many tissues [16,21–24]. The optical properties calculated for every mouse hindlimb with DOS were used as input for Eq. (4); thus blood flow estimates in both limbs were corrected for changes in absorption and scattering at every measurement point.

At each time point, the BFI for each source-detector separation in each hindlimb was estimated by the mean BFI across 120 time frames measured over an integration time of 500 ms each. The *perfusion ratio* was then defined as the ratio between the occluded and non-occluded limb BFIs, i.e., $Perfusion\ Ratio = BFI^{occluded} / BFI^{non-occluded}$. This parameter was used to quantify changes in perfusion over the whole experiment period.

In order to compare perfusion recovery in deeper regions of tissue with superficial perfusion dynamics, we also performed blood flow measurements with a commercial 1-channel LDF system (BPM 403A, TSI Inc., St. Paul, MN). The LDF probe, with a source-

detector separation of 500 μm , was used to obtain point measurements along a region of interest covered by the bottom portion of the DCS probe. We measured three different sites symmetrically positioned in each mouse hindlimb, and the average of the ratio between the three regions was compared to the perfusion ratio calculated with DCS.

2.4 Estimation of the metabolic rate of oxygen consumption

From measurements of HbO_2 , Hb , and HbT concentrations (the latter proportional to blood volume) and blood flow, the rate of oxidative metabolism can be indirectly assessed as the product of the rate of blood flow and relative oxygen extraction fraction (OEF). The OEF is defined as the fractional conversion of oxygen concentration from arterioles to venules. Assuming a steady-state balance between oxygen concentration and hemoglobin concentration, OEF can be written as the fractional change of oxygen saturation from arterioles (SaO_2) to venules (SvO_2) [34,35]. By employing a compartment model in which the optical signal originates from a mixture of arterial, capillary and venous blood, it is possible to write the tissue hemoglobin saturation measured directly from the optical signal (StO_2) as a sum of the different compartment saturations, which will lead to the following expression [34]:

$$OEF = \frac{S_a O_2 - S_t O_2}{\gamma S_a O_2}, \quad (5)$$

where γ indicates the percentage (fraction) of blood volume contained in the venous compartment of the vascular system. For measurements of relative changes and under the assumption of constant compartmentalization, the factor γ in Eq. (5) divides out. Typically, SaO_2 is obtained from blood gas measurements; in this work, we assumed SaO_2 was fixed at 100%, so that the relative metabolic rate of oxygen consumption (MRO_2) can be expressed as [36]:

$$\frac{MRO_2^{(oc)}}{MRO_2^{(no)}} = \frac{BFI^{(oc)}}{BFI^{(no)}} \frac{c_{Hb}^{(oc)} / c_{Hb}^{(no)}}{THC^{(oc)} / THC^{(no)}}, \quad (6)$$

where the superscripts (*oc*) and (*no*) in Eq. (6) refer to occluded and non-occluded limb, respectively.

3. Results

3.1 Physiological differences between mice genotypes

Figure 2 shows the perfusion ratio recovery curves for the two types of mice studied. At each time point in the figure, the marks are the median and the error bars represent the standard error across all the animals. Stars represent statistical significance difference between the two groups (ANOVA, $p < 0.05$). It is apparent that after inducing the same level of limb ischemia in both animals, KO mice recovered significantly less than control mice. Thus the role of $\text{HIF-2}\alpha$ in recovery of blood flow to overcome tissue hypoxia is demonstrated. While control mice were able to recover over 90% of their initial flow ratio (i.e., 90% of the ratio measured before femoral artery occlusion), KO mice reach a steady state level at approximately 55% of the initial flow levels. The rate of flow recovery also differs between the two animal groups; control mice respond faster and continuously to tissue hypoxia throughout the first weeks after occlusion.

Results from DOS measurements are shown in Fig. 3 for both occluded and non-occluded hindlimbs, and separated by animal types. Figure 3(a) shows the average absolute scattering coefficient at 785 nm across all mice obtained at every time point measured, assuming a homogeneous slab medium as previously discussed (Section 2.2). These values were used as inputs for DCS fitting so that the DCS-based perfusion ratios showed in Fig. 2 only reflect changes in blood flow. Figure 3(b) shows the absolute blood oxygen saturation obtained from

the absorption coefficient for all the time points measured. While oxygen saturation fluctuates around its mean initial value in the non-occluded limb during the whole 4-week period, oxygen saturation in the occluded limb goes down immediately after the femoral artery occlusion, and then slightly increases during the follow-up period. Regarding mouse type, KO mice present a significantly higher oxygenation deficit than controls, although both were unable to fully recover from their pre-surgery levels, in contrast to blood flow recovery. No differences were seen in the non-occluded limb as a function of mouse type, as expected.

The absolute levels of total hemoglobin concentration are plotted in Fig. 3(c). Before any intervention, HbT concentration was measured as approximately 70 μM in both hindlimbs. This level remained constant in the non-occluded limb over the whole period. On the other hand, hypoxia induced an increase of 26% in total hemoglobin concentration in the occluded limb after 4 weeks for both types of animals. This increase may be related to the formation of new vessels within the tissue.

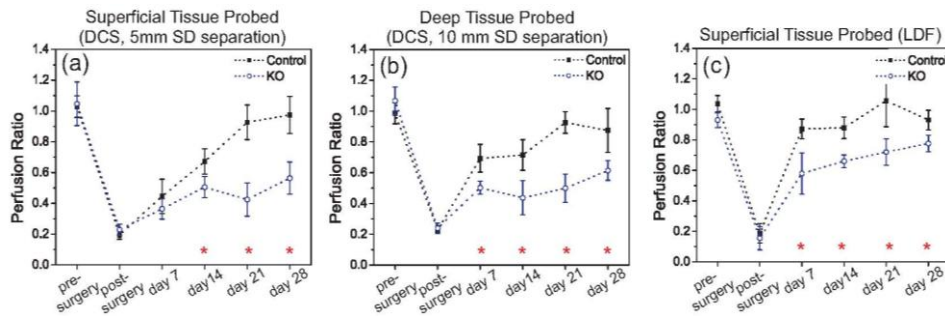


Fig. 2. Median perfusion ratio calculated from all the survival mice, separated by mice genotype. Data were collected at (a) 5 mm and (b) 10 mm source-detector separations with DCS, and (c) with LDF. Error bars represent the standard error across the animals, and the stars are the time points with statistical difference between the two mice genotypes (ANOVA, $p < 0.05$).

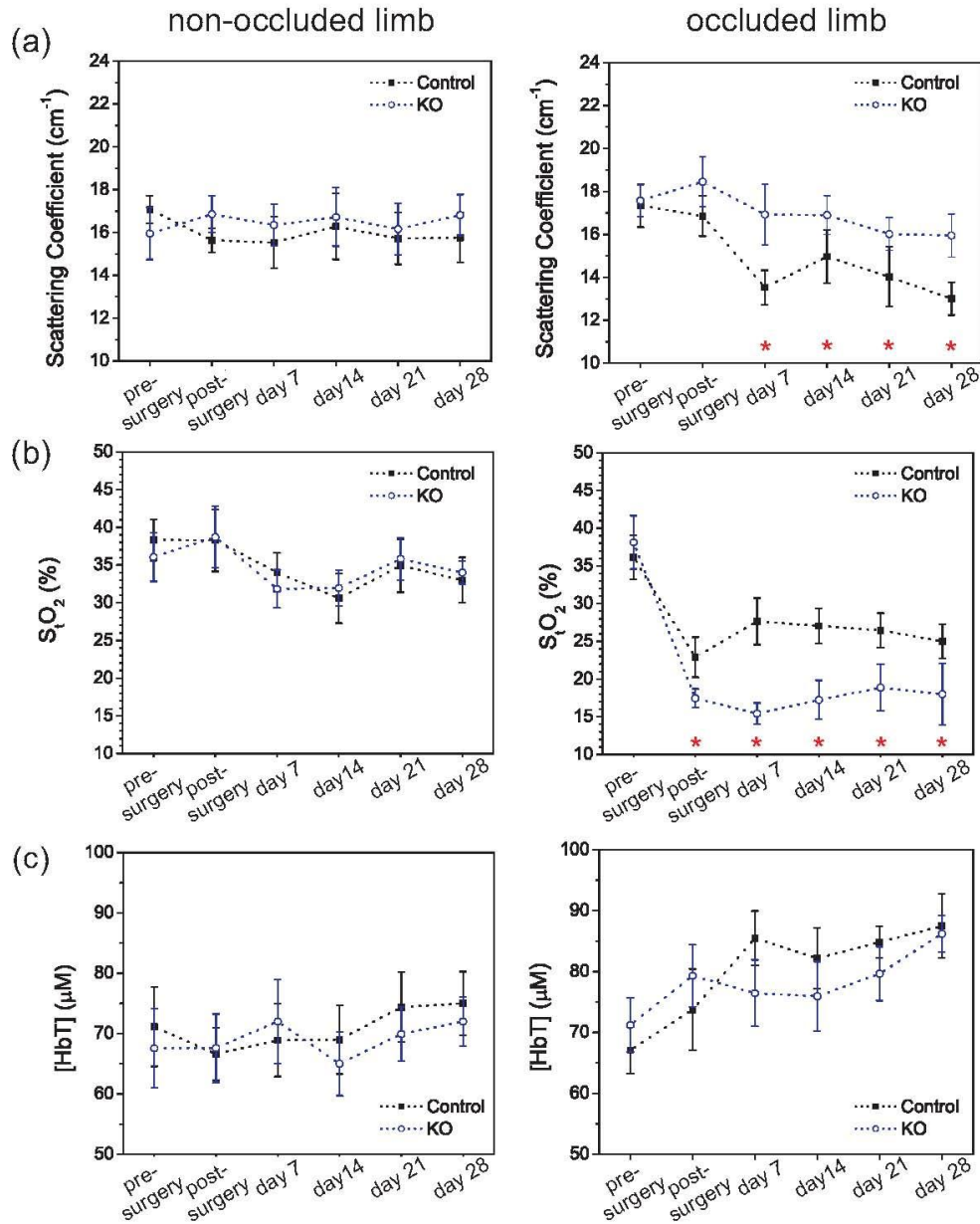


Fig. 3. (a) Absolute scattering coefficient at 785 nm, (b) tissue oxygen saturation and (c) THC in the limb calculated from all the survival mice, separated by mice genotype, for both the non-occluded and occluded hindlimbs. Error bars represent the standard error across the animals, and the stars denote the time points with statistical difference between the two mice genotypes (ANOVA, $p < 0.05$).

3.2 Histological analysis

Recovery of flow is related to the angiogenesis process induced by tissue hypoxia after femoral artery occlusion. Histological slices from the occluded hindlimbs taken 28 days after artery ligation show a completely different vascular network, with a significant increase in vessel/capillary density in the abductor muscle. An example of such difference can be seen in Fig. 4, which shows a representative field of a portion of the abductor muscle from a single

mouse, in which the vessels/capillaries were marked with rhodamine. While the average vascular density in the non-occluded limb was $(0.98 \pm 0.11)\%$ for both types of mice, the occluded limb of KO mice presented an average vascular density of $(3.9 \pm 0.3)\%$. This number was even higher in control mice, $(6.1 \pm 0.2)\%$.

3.3 Reperfusion profile across the limb

Temporal dynamics following artery ligation presented the same generic trends for all animals studied and were very similar at the two DCS source-detector separations. The same pattern, shown in Fig. 2 for DCS, was also seen for superficial flow measured by LDF, suggesting that blood flow recovers at all levels within the tissue. The amount of recovery, however, was different and depended on the depth of the tissue. Because DCS and LDF probe different depths of tissue below the surface, and because the formation of new vessels leads to differences in the vascular network across the limb, direct comparison between the two techniques is not straightforward.

Figure 5 relates DCS and LDF findings to histological results from the most superficial part of the muscle (denoted superficial in Fig. 5) and from tissue about 4 mm deep into the muscle (denoted deep in Fig. 5). For data points collected pre- and post-surgery, both of the DCS source-detector separations are highly correlated with LDF (i.e., correlation greater than 0.8), with slope close to unity (i.e., $DCS/LDF = (0.96 \pm 0.10)$ for 5 mm and (1.07 ± 0.08) for 10 mm SD separation, respectively). Such a strong linear relationship suggests that the limb is uniformly perfused before intervention, and that it remains uniformly perfused – at a lower level – just after the femoral artery occlusion. This observation is in agreement with histological findings in the non-occluded limb, which can be used to indirectly assess the pre-surgery condition. Taken together, these results provide another source of validation for DCS as a technique that can reliably provide a blood flow index proportional to *in vivo* tissue blood flow.

On the other hand, when the correlation between DCS and LDF is taken with data collected at 7, 14, 21, and 28 days post-surgery, the correlation drops to $0.30 (\pm 0.04)$, suggesting that the formation of new vessels occurs in a different manner across the limb. The slopes of the DCS versus LDF correlation curves (DCS/LDF) are measurably less than unity, indicating heterogeneity in tissue response. The slope of the DCS versus LDF correlation curve decreases slightly from the 5 to the 10 mm SD separation ($DCS/LDF = (0.69 \pm 0.22)$ for 5 mm SD separation, and (0.46 ± 0.18) for 10 mm SD separation), and thereby provides slightly more evidence for the existence of a gradient in the recovery of blood flow from superficial to deeper tissue wherein more superficial tissue is reperfused faster. Indeed, histological slices from the adductor muscle confirm that the superficial tissue in the occluded limb is more vascularized than the deep tissue after 28 days, again providing evidence of the origin of higher perfusion ratios of LDF compared to DCS.

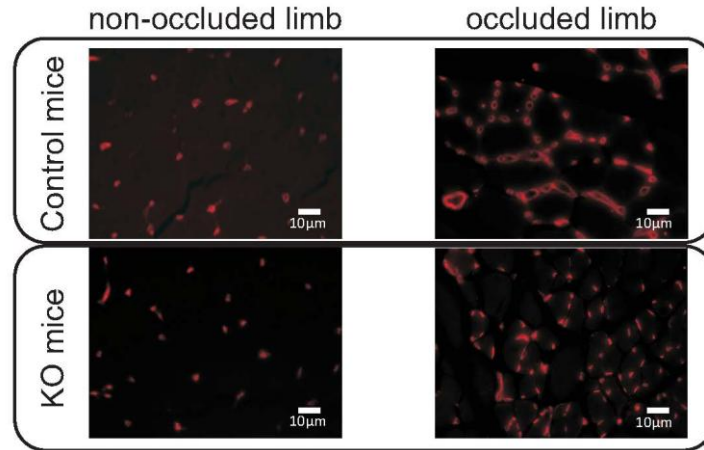


Fig. 4. Representative field in the adductor muscle showing Rhodamine-labeled vessels/capillaries in the non-occluded and the occluded limb from control and KO mice, obtained 28 days after femoral artery ligation.

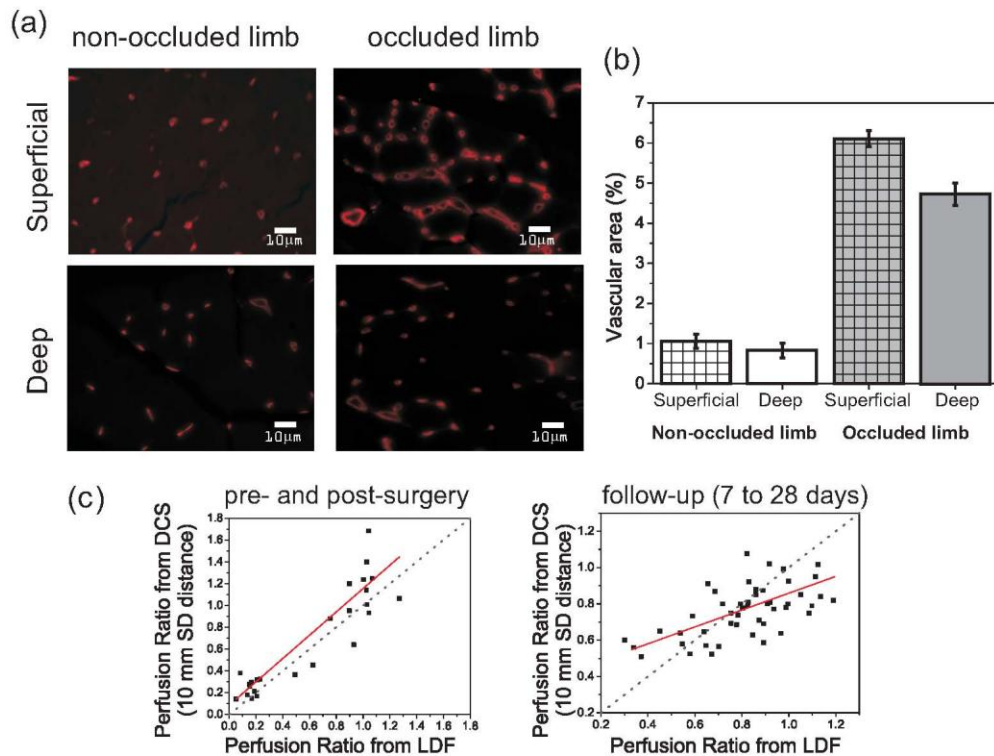


Fig. 5. (a) Vessel/capillary density and vascular area in an adductor muscle specimen from a control mouse 28 days after femoral artery ligation. Vasculature was visualized using a Rhodamine Lectin staining. Images were taken at the most superficial part (labeled superficial) of the muscle, immediately under the skin, and approximately 4 mm into the muscle (labeled deep). (b) Quantification of superficial and deep vascular area for both the non-occluded and occluded limbs in control mice. (c) Comparison of the perfusion ratios obtained via DCS (10 mm source-detector separations) to LDF measured perfusion ratios. The plot on the left contains data from pre- and post-surgery, while the one in the right shows data from the follow-up measurements. The gray line indicates a unity slope for $\text{Perfusion Ratio}_{\text{DCS}}/\text{Perfusion Ratio}_{\text{LDF}}$, while the red line shows the best linear fit to the data.

3.4 Metabolic recovery of the tissue

One of the potential advantages for measuring microvascular blood flow and oxygenation with diffuse optical methods is the possibility of estimating the tissue consumption of oxygen indirectly from the hemodynamic parameters, thus providing metabolic information. Figure 6 shows the metabolic rate of oxygen in the occluded limb, as a fraction of the non-occluded one. As blood flow responds to tissue demand, trends for MRO_2 follow the ones found for blood flow ratio. The metabolic response to hypoxia was shown to be fast, recovering about 30% in the first 7 days. Regarding mice type, we found that deletion of *HIF-2 α* presented a long-term effect, i.e., KO mice were unable to recover more than 60% of their initial metabolism. Control mice fully recovered their initial oxygen consumption ratio in 3 weeks.

4. Discussion

This work aimed to verify the feasibility of diffuse correlation and diffuse optical spectroscopies as monitoring tools for characterizing angiogenesis processes longitudinally in murine models *in vivo*. By performing femoral artery ligation in a mouse hindlimb, both DCS and DOS were shown to reliably monitor physiological recovery due to induced tissue hypoxia, i.e., despite inter-mouse variability caused by mouse physiology, different responses to anesthesia and to femoral artery occlusion. For both perfusion and oxygenation, we found the variability to be about 25-30% from the mean values in each group at each time point.

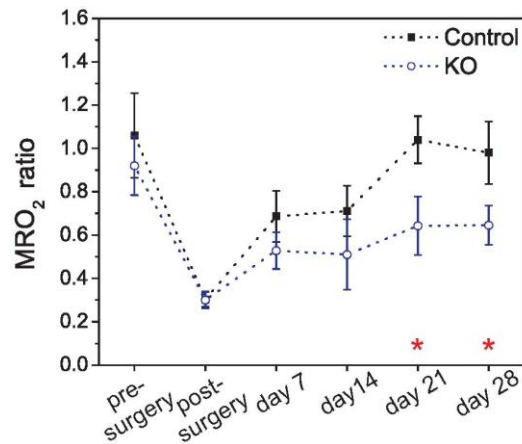


Fig. 6. Metabolic rate of oxygen consumption ratio in the limb for all the time points measured, and separated by mice genotype. Error bars represent the standard error across all the animals, and the stars denote the time points with statistical difference between the two mice genotypes (ANOVA, $p < 0.05$).

The intra-mouse variability was mostly related to techniques and was lower than inter-mouse variability. For example, for the nine different locations measured with DOS in each limb at each time point, the variance was smaller than 17% of the mean value in every mouse. The variance was even smaller when computed over the 120 frames acquired with DCS (i.e., it ranged from 1.8% to 8.5%). Both measurement types were sensitive to differences related to mice genotype, which permitted comparison between different mice types. In particular, a larger perfusion and oxygen saturation recovery was observed in control mice compared to KO mice. The perfusion ratio curves of recovery measured by DCS are very similar to curves reported in previous studies of hindlimb ischemia models in control mice with LDF/LDI [6,14], and they also agree with recent findings in mice bearing mutations in the *HIF-1 α* gene, which is known to encode a transcription factor important in the angiogenesis process [14].

Despite the successful application of both DCS and DOS analysis in this problem, the limitations of analytical solutions can be questioned, especially given the small dimensions involved. Furthermore, by contrast to most of the DCS studies reported in the literature thus far, which use the solution of the diffusion equation for the semi-infinite geometry [21–24],

we compared data to solutions in the slab geometry to achieve better accuracy (Section 2.3). A comparison of results between the two approaches, however, yielded less than 5% difference. We also performed Monte Carlo simulations assuming a homogeneous medium, and fit the correlation curves obtained from the recorded pathlength in the simulation [37,38]. Again, differences between analytical solutions and Monte Carlo simulations were within the error bars of Fig. 2. Table 1 compares the perfusion rates obtained by three different analysis approaches.

Unlike LDF/LDI, the intrinsic capability of diffuse optical methods to probe deep tissues enabled us to monitor physiological responses due to femoral artery occlusion at different depths in the limb. Although the perfusion dynamics following ischemia was very similar in superficial tissues (as measured by LDF) and deeper tissues (as measured by DCS), the correlation of perfusion ratios between these two techniques decreased approximately 50% relative to the correlation ratio prior to injury [Fig. 5(c)]. Since the techniques are sensitive to blood flow at different positions in the tissue, this result suggests that the new vessel formation induced by femoral artery ligation leads to a non-uniform vascular network, in which superficial tissues experience greater reperfusion than deeper tissues. Histological observations supported this model: the sprouting and formation of capillaries from the pre-existing vasculature is more prominent in superficial tissues relative to deeper regions. The angiogenic process has a limited capacity to increase perfusion in the surrounding ischemic tissue [39]. Another factor in reperfusion is the arteriogenic process, defined as the

Table 1. Perfusion Ratio calculated by three different approaches from DCS data from control mice, separated by source-detector separation. Uncertainty of the values denotes the standard error across all animals

Method	Perfusion Ratios					
	Pre-surgery	Post-surgery	Day 7	Day 14	Day 21	Day 28
5 mm SD separation						
Slab solution	1.03 ± 0.06	0.19 ± 0.02	0.45 ± 0.08	0.67 ± 0.08	0.93 ± 0.09	0.97 ± 0.10
Semi-infinite solution	1.03 ± 0.07	0.19 ± 0.03	0.44 ± 0.08	0.68 ± 0.09	0.94 ± 0.09	0.97 ± 0.10
Monte Carlo	1.13 ± 0.05	0.22 ± 0.03	0.41 ± 0.07	0.59 ± 0.07	0.85 ± 0.10	0.91 ± 0.08
10 mm SD separation						
Slab solution	0.98 ± 0.06	0.23 ± 0.02	0.69 ± 0.08	0.71 ± 0.09	0.91 ± 0.06	0.88 ± 0.14
Semi-infinite solution	0.97 ± 0.08	0.24 ± 0.03	0.71 ± 0.09	0.72 ± 0.10	0.91 ± 0.07	0.90 ± 0.12
Monte Carlo	1.11 ± 0.05	0.25 ± 0.01	0.61 ± 0.08	0.65 ± 0.10	0.85 ± 0.07	0.91 ± 0.06

enlargement and proliferation of pre-existing collateral arteries and their remodeling into effective conductance vessels [40]. Therefore, in response to ligation of the deep femoral artery, blood flow may increase in superficial collateral arteries leading to the differences in reperfusion observed between superficial and deeper tissues.

Tissue oxygen saturation obtained from DOS measurements showed the same recovery trend as perfusion. Regarding absolute quantification and the apparently low absolute blood oxygen saturation, it is important to note that the oxyhemoglobin dissociation curve of mice is significantly shifted compared to that of humans. This shift effectively yields comparatively lower oxygen saturations in mice compared to humans for the same values of oxygen partial pressure [41,42]. The observed range of 32 to 44%, obtained before femoral artery occlusion, is therefore consistent with previous reports for this population [42–44]. Regarding genetic background, we found that KO mice presented a higher oxygenation deficit than controls [Fig. 3(b)]. Interestingly, although control mice recover 95% of their initial perfusion, their limb oxygen saturation only reached 75% of pre-ligation levels. The reduction in blood oxygen saturation, in spite of a marked recovery of flow, may be attributed to a new but less efficient vascular network. The new vessels, which form during angiogenesis, are predominantly capillaries. These newly formed capillaries are effectively endothelial cell tubes, which lack well developed wall structures and exhibit a limited capacity for blood flow [39]. In addition, new vessels tend to be leakier, especially in KO mice, and this may account for significantly smaller oxygen consumption in mutant mice compared to controls (Fig. 6).

In order to estimate the rate of oxygen consumption we assumed that the percentage of blood volume contained in the venous compartment of the vascular system is the same for both limbs [Eq. (6)]. In addition, SaO_2 was fixed at unity for both limbs at all time points. These assumptions do not hold after ligation of the femoral artery, since the main entrance of blood flow to the occluded limb is blocked. Despite the lack of information on the longitudinal values of these parameters, a variation in SaO_2 in the occluded limb from 70% to 100% would produce a variation of less than 3% in the final MRO_2 estimation. A further careful analysis using blood gases to provide direct measurements of SaO_2 , for example, would provide a more accurate estimation of oxygen consumption, and will be the subject of future publications.

In summary, DCS and DOS are shown to be feasible methods to assess physiology in animal models of angiogenesis. By noninvasively probing the tissue, it is possible to monitor perfusion rates and oxygenation over long periods of time without sacrificing a subset of animals for histological analysis at each time point. Based on studies in mice with endothelial cell-specific deletion of *HIF-2 α* , diffuse optical methods were able to quantify differences in animals with very different angiogenic properties. The combination of these two diffuse optical methods allowed a more complete characterization of the tissue dynamic processes in response to angiogenesis induced by hindlimb ischemia. The ability to probe deep tissues allowed us not only to quantify the dynamics of neoangiogenesis across the whole tissue, but also to discuss distinctions between superficial and deep regions of limb muscle. Lastly, acquisition of both blood flow and oxygenation allows for an indirect estimate of oxygen metabolism from hemodynamics, thereby providing more direct information of the underlying tissue.

5. Conclusions

The main contribution of the present research is its establishment of diffuse optics as a noninvasive and practical method to evaluate the role of transcription factors in mice physiology; diffuse optics permits investigation of HIF-2 α effects to be carried out with improved features, i.e., study of the whole limb with more physiological parameters. By combining DCS and DOS to determine blood flow and oxygenation responses of the tissue, we were able to noninvasively monitor physiological variations during angiogenesis induced by hindlimb ischemia in a mouse model. The revascularization process initiated by angiogenesis was found to reestablish perfusion and oxygen consumption after four weeks in control mice. The vascular recovery of mice with endothelial-specific deletion of HIF-2 α was significantly impaired relative to control mice, indicating the importance of this gene for endothelial cell functions in angiogenesis. Perfusion measurements obtained with DCS compared with blood flow measurements performed with LDF showed a significant correlation between the two techniques before femoral artery occlusion. This correlation decreases significantly during angiogenesis due to differences in the formation of new vessels according to tissue depth. Histological analysis performed after 28 days match physiological findings. In summary, the combined optical measurements of both DCS and DOS enabled better understanding of the interplay between perfusion, oxygenation concentration, and oxygen metabolism during murine angiogenesis.

Acknowledgments

The authors would like to thank Regine Choe and Joel Greenberg for helpful discussions and feedbacks, and Zachary Quinn for technical assistance. This work was supported by the National Institutes of Health (R01-NS060653, HL66130, and RR02305), and the Howard Hughes Medical Institute.